

**Preliminary Implementation of Improved Heat Transfer and  
Impingement-Direction Ice Growth Modeling in Numerically  
Simulated Ice Accretion (LEWICE/X)**

by

Matthew T Velazquez

B.S., Aeronautics and Astronautics  
Massachusetts Institute of Technology, 1993

Submitted to the Department of Aeronautics and Astronautics in partial  
fulfillment of the requirements for the degree of

Master of Science in Aeronautics and Astronautics

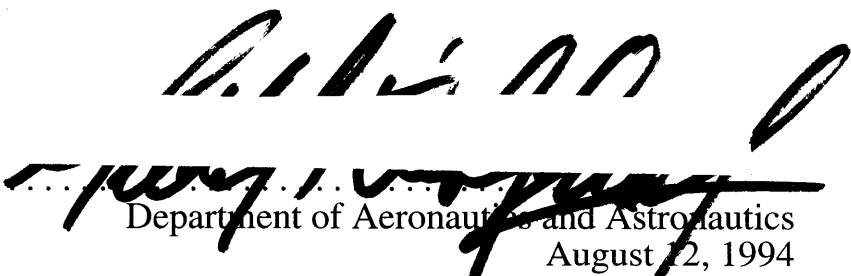
at the

MASSACHUSETTS INSTITUTE OF TECHNOLOGY


September 1994

© Massachusetts Institute of Technology 1994. All rights reserved.

Author .....

  
Department of Aeronautics and Astronautics  
August 22, 1994

Certified by .....

  
R. John Hansman  
Associate Professor  
Thesis Supervisor

Accepted by .....

  
Prof. Harold Y. Wachman  
Chairman, Department Graduate Committee

MASSACHUSETTS INSTITUTE  
OF TECHNOLOGY

SEP 21 1994

LIBRARIES

Aero

**Preliminary Implementation of Improved Heat Transfer and  
Impingement-Direction Ice Growth Modeling in Numerically Simulated  
Ice Accretion (LEWICE/X)**

by

Matthew T Velazquez

Submitted to the Department of Aeronautics and Astronautics  
on August 12, 1994, in partial fulfillment of the  
requirements for the degree of  
Master of Science in Aeronautics and Astronautics

**Abstract**

Experimental observations have shown that discrete rime ice growths called feathers, which grow in approximately the direction of water droplet impingement, play an important role in the growth of ice on accreting surfaces for some thermodynamic conditions. An improved physical model of ice accretion has been implemented in the LEWICE 2D panel-based ice accretion code maintained by the NASA Lewis Research Center. The LEWICE/X model of ice accretion explicitly simulates feather growth within the framework of the LEWICE model. Water droplets impinging on an accreting surface are withheld from the normal LEWICE mass/energy balance and handled in a separate routine; ice growth resulting from these droplets is performed with enhanced convective heat transfer approximately along droplet impingement directions. An independent underlying ice shape is grown along surface normals using the unmodified LEWICE method. The resulting dual-surface ice shape models roughness-induced feather growth observed in icing wind tunnel tests. Experiments indicate that the exact direction of feather growth is dependent on external conditions. Data is presented to support a linear variation of growth direction with temperature and cloud water content. Test runs of LEWICE/X indicate that the sizes of surface regions containing feathers are influenced by initial roughness element height. This suggests that a previous argument that feather region size is determined by boundary layer transition may be incorrect. Simulation results for two typical test cases give improved shape agreement over unmodified LEWICE.

Thesis Supervisor: R. John Hansman  
Title: Associate Professor

# Contents

<b>1 Introduction</b>	7
1.1 Motivation for Icing Studies	7
1.2 Factors in Ice Accretion	8
1.3 Types of Ice Accretions	9
1.4 Role of Roughness and Feathers in Icing	11
<b>2 Numerical Icing Simulation</b>	14
2.1 Current Research	14
2.2 Basic LEWICE Structure	16
2.3 Physical Modeling of Ice Growth	18
2.4 LEWICE Performance and Models	20
<b>3 LEWICE/X</b>	21
3.1 Physical Basis for Code Modification	21
3.1.1 Heat Transfer Considerations	21
3.1.2 Feather Growth Direction	22
3.2 Description of Improved Ice Growth Model	23
3.2.1 Thermodynamic Calculations	25
3.2.2 Feather Growth	27
3.2.3 Substrate Growth	28
3.2.4 Calculation of Iced Geometry	29
3.3 LEWICE/X Performance	34
3.3.1 Summary	31
3.3.2 Observations of LEWICE/X Performance	32
<b>4 Conclusions</b>	39
4.1 Summary	39
4.2 Observations of LEWICE/X Performance	40

# List of Figures

Figure 1. Definitions of local and global collection efficiency .....	9
Figure 2. Ice types .....	10
Figure 3. Ice shape types .....	11
Figure 4. Photograph of rime feathers .....	11
Figure 5. Roughness-enhanced heat transfer and feather growth .....	12
Figure 6. Photograph of Type A horns .....	13
Figure 7. Non-feather modes at potential feather nucleation sites .....	13
Figure 8. Flowcharting for LEWICE .....	17
Figure 9. Mass balance for a typical control volume .....	18
Figure 10. Results of feather growth angle analysis .....	22
Figure 11. Feathers modeled as a continuous surface .....	23
Figure 12. Flowcharting for LEWICE/X .....	24
Figure 13. Solidity definition .....	25
Figure 14. Feather vs. substrate growth directions .....	27
Figure 15. Initial repaneling method for feather geometry .....	30
Figure 16. Illustration of panel anomaly inherent to numerical method .....	31
Figure 17. New feather shape point distribution method .....	33
Figure 18. Feather-substrate panel correspondence .....	33
Figure 19. Solidity sweep for parameters of Figure 20 .....	34
Figure 20. Roughness sweep for parameters of Figure 20 .....	35
Figure 21. Accretions on 3.5" diameter cylinders. V=200 mph; LWC=0.32 g/m <sup>3</sup> ; MVD=15 m; Temp.=25°F. 12 minute accretion. ....	36
Figure 22. Accretions on 3.5" diameter cylinders. V=200 mph; LWC=0.5 g/m <sup>3</sup> ; MVD=15 m; Temp.=25°F. 12 minute accretion. ....	37

# Nomenclature

$\dot{m}_c$ : mass flux impinging

$\dot{m}_e$ : mass flux evaporating

$\dot{m}_i$ : mass flux freezing out

$\dot{m}_{rin}$ : runback mass flux in

$\dot{m}_{rout}$ : runback mass flux out

$f$ : freezing fraction of impinging and runback mass

$q_{impinging}$ : heat transfer due to impinging mass

$q_{evaporating}$ : heat transfer due to evaporating mass

$q_{freezing}$ : heat transfer due to freezing mass

$q_{runback,in}$ : heat transfer due to runback in

$q_{runback,out}$ : heat transfer due to runback out

$q_{conduction}$ : heat transfer due to conduction

$q_{convection}$ : heat transfer due to convection

$\Delta s$ : segment length

$q_k$ : conductive heat transfer per unit length

$HTC$ : convective heat transfer coefficient

$V_\infty$ : free stream velocity

$V_e$ : velocity at the edge of the boundary layer

$C_{p(w,s)}$ : Specific heat of water at edge temperature

$C_{pw,sur}$ : Specific heat of water at surface temperature

$C_{pi,sur}$ : specific heat of ice at surface temperature

$L_v$ : latent heat of vaporization

$L_f$ : latent heat of fusion

$T_s$ : static temperature in free stream

$T_{sur}$ : surface static temperature

$T_m$ : melting temperature

$\dot{m}_f$ : mass flux of impinging water onto feather panel

$\dot{m}_s$ : mass flux of impinging water onto substrate panel

$f_f$ : freezing fraction for feather panel

$f_s$ : freezing fraction for substrate panel

$e$ : heat transfer enhancement factor

$\sigma$ : feather region solidity

$h_{feather}$ : projection of feather length onto surface normal

# Chapter 1

## Introduction

Icing has been a topic of major concern in the aviation community for the past several decades [9]. The aerodynamic performance degradation associated with ice accretions on wings, intakes, rotors, propellers, and other flying surfaces has prompted research into the physics of ice accretion and the development of many anti-/de-ice technologies. The ability to predict the icing performance of various configurations has improved greatly in the last fifteen years, mainly due to the development of several icing simulation codes [10]. These codes, based on theoretical and empirical flowfield, particle trajectory, and heat transfer models, reduce the time and money required for actual icing certification tests, both in flight and in icing wind tunnels.

### 1.1 Motivation for Icing Studies

Ice accretes on an aircraft when it passes through a cloud of supercooled water droplets. The resulting ice shape is dependent on external and local thermodynamic conditions, airspeed, particle size and density, and the specific geometry of the accreting surface. The presence of ice on an aircraft's lifting and control surfaces can degrade its aerodynamic performance. Even a very small amount of ice on the leading edge of a wing or tailplane can significantly alter the airflow, causing loss of lift or of control surface

effectiveness in critical situations.

## 1.2 Factors in Ice Accretion

There are several fundamental parameters that govern the ice accretion process and ultimately determine the type and extent of the ice accretion. They are:

- **Airspeed.**
- **Air temperature.**
- **Cloud liquid water content (LWC)**, usually in  $\text{g/m}^3$ .
- **Mean volumetric diameter (MVD)**, the mean size of the incoming droplet distribution.
- **Configuration geometry.**

In addition to the above parameters, there are several common quantities that aid in the characterization of an icing encounter for a particular configuration:

- **Impingement limits.** These are the aftmost locations on the surface where incoming droplets impinge on the surface. Their exact positions move as the geometry changes during an icing encounter.
- **Collection efficiency,  $\beta$ .** This characterizes the configuration's ability to capture incoming water, and can be defined locally or globally for the entire configuration. It is defined as the ratio of upstream vertical separation between two particles to the distance along the surface between their impact points. Local and global definitions are presented for an airfoil section in Figure 1.
- **Freezing fraction,  $f$ .** This is the percentage of incoming water that freezes during the icing encounter. Like the collection efficiency, freezing fraction can be defined locally or globally.

Local definitions of  $\beta$  and  $f$  will be used in subsequent calculations.



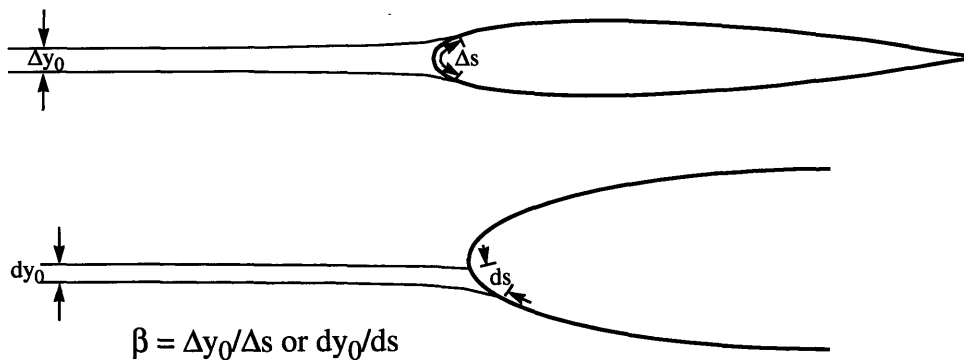


Figure 1. Definitions of global and local  $\beta$ .

### 1.3 Types of Ice Accretions

Different combinations of the above parameters will result in the formation of different types of ice. The principal types are detailed below (Figure 2).

- *Rime ice*: opaque or milky in color, rime ice forms at lower temperatures and at low LWC. When the temperature is low enough, incoming droplets freeze on impact, creating small air pockets in the ice shape that give rime ice its opacity and lower its density. Because the freezing fraction for rime ice is high, it is referred to as “dry growth”.

- *Glaze ice*: characterized by its transparency and high density, it is formed at temperatures close to freezing and at high LWC. Glaze ice grows when the local freezing fraction is low, resulting in the presence of unfrozen water on the accreting surface during the icing encounter. Because of this glaze accretion is sometimes referred to as “wet growth”. Often in glaze accretions large horns grow away from the surface due to the relatively high heat transfer aft of stagnation. These are Type B or “wet” horns (Figure 3).

- *Mixed ice*: in some conditions the local heat transfer at an accreting surface is

such that the freezing fraction is low at stagnation but increases aft. This causes the simultaneous formation of rime ice aft of stagnation and glaze in the center. The resulting ice shape is called a mixed accretion. Horn formation also occurs in these conditions. Hansman et. al [1] identified the mixed horn, designated Type A (Figure 3). Generally smaller than wet horns, these form when rime growths aft of stagnation are “backfilled” with runback water from upstream. Type A horns grow roughly in the droplet impingement directions, or “into the flow”, and are directly related to the growth of rime ice “feathers” that had been noted previously in colder accretions. Type A horns and the mechanisms by which they form are the physical basis for this thesis and are detailed in Section 1.4.

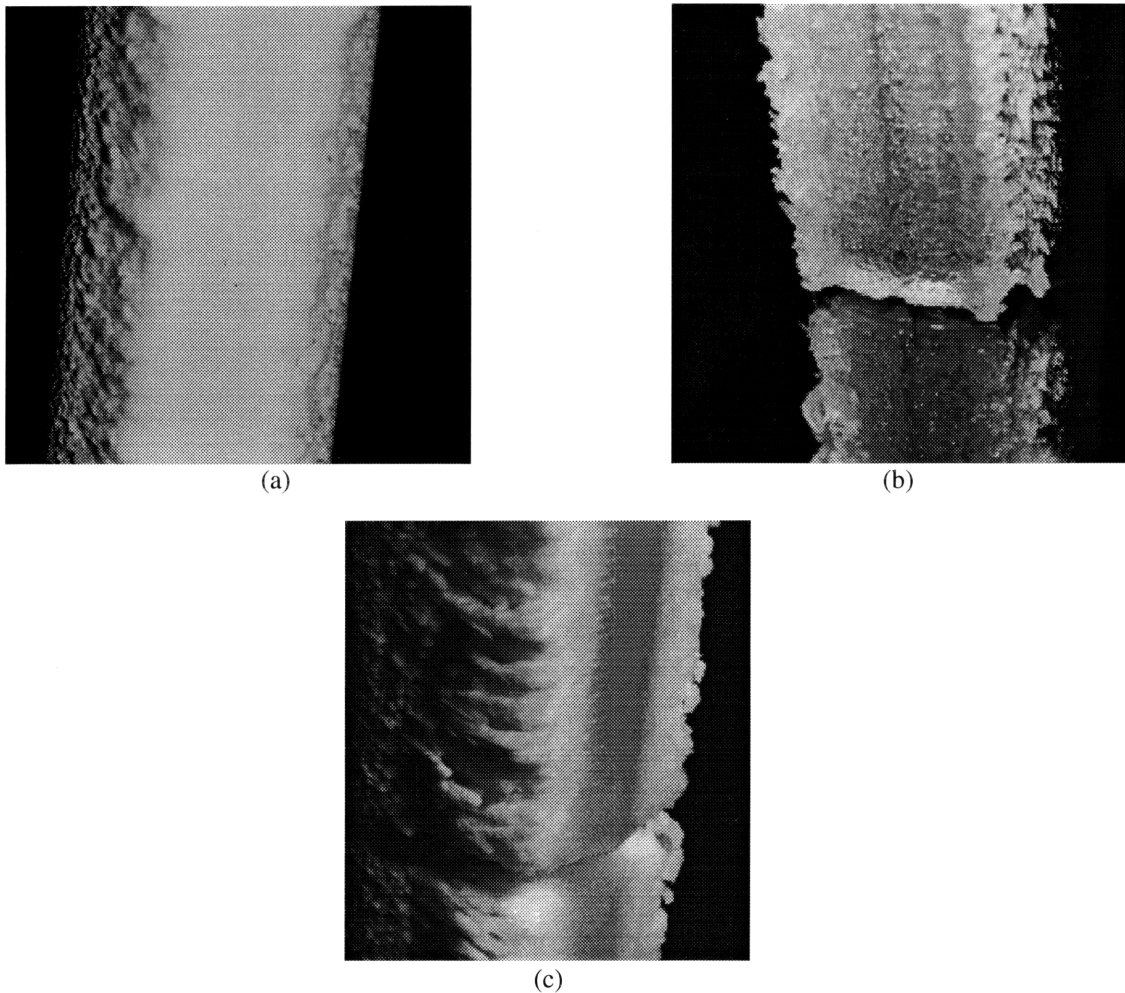


Figure 2. Ice types. Accretions are on a 3.5” diameter cylinder. (a) Rime ice. Flow is into the page. (b) Glaze ice with shape tracing cutout. Flow is into the page and to the right. (c) Mixed ice with shape tracing cutout. Flow is to the left and into the page.

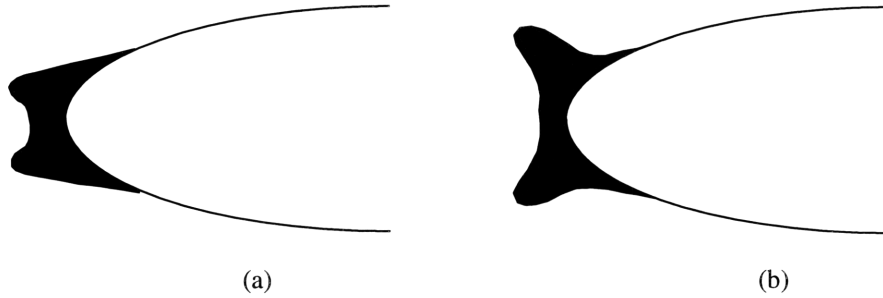


Figure 3. Ice shape types. (a) Horn A; (b) Horn B.

## 1.4 Role of Roughness and Feathers in Icing

It is well known that surface roughness plays a pivotal part in boundary layer development. Since the boundary layer state determines the local convective heat transfer at the surface, roughness also plays a very important role in ice growth for any conditions by determining the transition location. For some conditions, the presence of small roughness elements on an accreting surface can also affect the iced geometry by nucleating rime “feathers”. These are small discrete rime growths that first appear in all but pure glaze conditions and grow in the direction of local impingement. They are fan-shaped, with opening angles of  $20^\circ$  to  $50^\circ$ , and are roughly aligned with the mean chord plane (Figure 4).

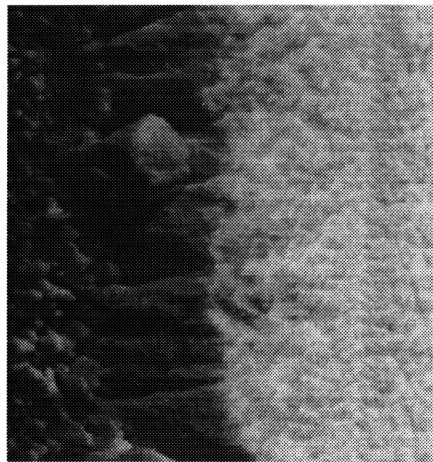


Figure 4. Rime feathers at the edge of a rime accretion. Flow is to the left.

In [2] it was shown that (a) feathers grow from initial surface contamination sites and propagate into the flow, and (b) small roughness elements have enhanced convective heat transfer properties that allow feather growth to initiate (Figure 5).

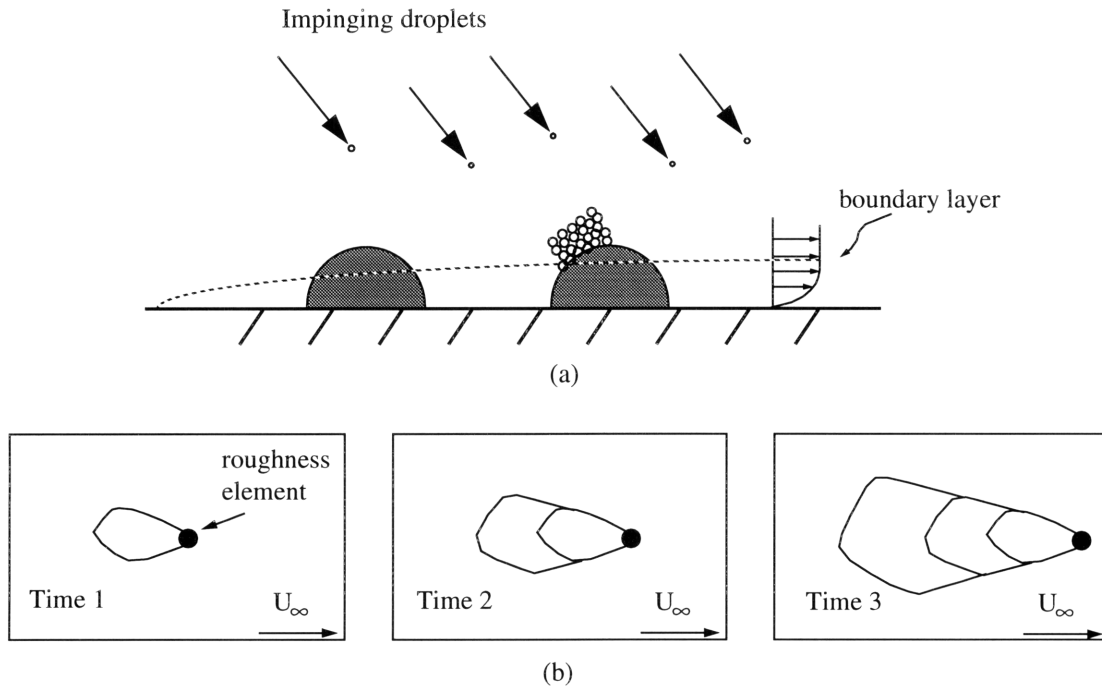


Figure 5. Roughness-enhanced heat transfer and feather growth. (a) Enhanced heat transfer at element tips allows them to freeze incoming droplets more readily than a smooth surface. Element on the right has begun to accrete. (b) Snapshots of feather growth, top view.

The high heat transfer at a contamination site causes droplets impacting there to freeze immediately upon impact. This increases the contaminant's size and extends it closer to the boundary layer edge. Large elements can grow out of the boundary layer altogether and become individual miniature collectors. This process results in the formation of feathers on the surface and, if enough feathers grow close together, Type A horns such as those shown in Figure 6.

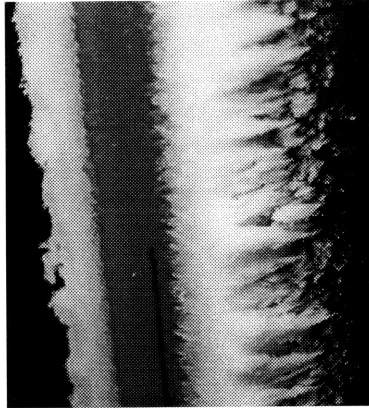


Figure 6. Type A horns aft of glaze stagnation zone. Flow is to the right into the page.

It is notable that there are no feathers in the stagnation region in this figure, nor in any mixed accretions. Based on observations of close-up video, two physical mechanisms for this phenomenon have been identified (Figure 7). The flow conditions may be such that the local heat transfer is not high enough to freeze all impacting droplets immediately at roughness sites. In this case the roughness is smoothed over by incoming water and no feathers are grown. Runback water from upstream locations may also prevent feather nucleation by washing over roughness elements, partially or completely covering them. This not only reduces convective heat transfer but also reduces the total amount of water freezing at the roughness site by surrounding it with a relative heat sink. This mechanism can prevent feather growth from a roughness element even though the heat transfer at the dry element tip was high enough to grow feathers.

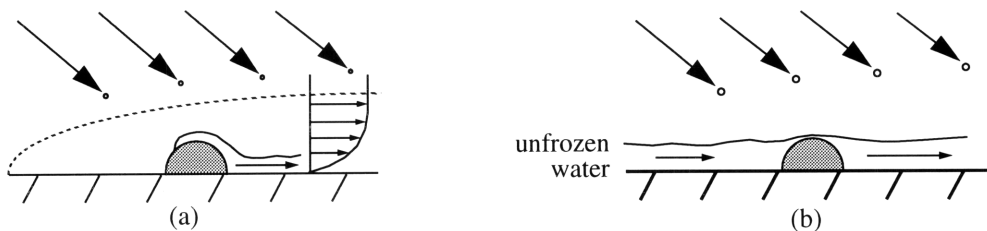


Figure 7. Non-feather modes at potential feather nucleation sites. (a) Low heat transfer. Droplets fail to freeze on roughness and run back along surface. (b) Unfrozen water overgrowth. Heat transfer is reduced when roughness element is covered by glaze runback.

# Chapter 2

## Numerical Icing Simulation

In order to develop an effective anti-ice or de-ice system, a designer must first determine where, to what extent, and how readily an aircraft's surfaces will accrete ice. Portions of an aircraft configuration, such as a flush-mounted antenna or an engine nacelle, may require special attention with respect to icing performance. It is therefore advantageous to input the geometry into an icing simulation code and use the resulting numerical predictions as guides in the design of an icing protection system or a test matrix for tunnel icing tests. This can reduce significantly the time required for design finalization and certification.

### 2.1 Current Research

Icing simulation is very much an ongoing endeavor. Even though icing has been a major design and operational issue since the 1940s, researchers still have only a limited understanding of the mechanisms behind the numerous phenomena that influence ice growth. This is particularly true for glaze and mixed ice growth regimes. Since the publication of [10], many new physical models and code suites have been developed. Two-dimensional and three-dimensional codes have been implemented. Most ice accretion simulation programs are structurally similar. For example, all ice accretion codes have a four-step accretion procedure:

**Step 1:**Determine the flow field for current geometry;

**Step 2:** Calculate drop trajectories and collection efficiency distribution;

**Step 3:** Perform energy analysis to determine ice thickness distribution;

**Step 4:** Update iced surface geometry.

Specific flowfield and trajectory models differ from code to code, but most use variations of Messinger's control volume model for computing the ice growth [7], detailed in Section 2.3. The NASA Lewis Research Center in Cleveland, Ohio, has developed a number of codes under the common name LEWICE, which has been distributed to U.S. companies and universities for design and research purposes. There are several different varieties of the base code, each with different capabilities.

- **LEWICE.** A potential flowfield/integral boundary layer module attached to a trajectory integration code and a Messinger-model ice growth code. The fourth major revision of this code, called the “Beta” version, is the most recent release and is being distributed by NASA LeRC as of this writing. It is capable of performing ice accretions on multiple bodies. The simple flowfield solution method allows short computation times but does not capture separations and can give inaccurate flowfield predictions for complex shapes. 2D and 3D versions of this code exist.

- **LEWICE/NS.** A C-grid based Euler/Navier-Stokes flowfield calculator with accompanying modifications to the trajectory and ice growth modules. Intended as a research tool, the flow solver captures flow separations and can predict steady and unsteady aeroperformance of 2D iced airfoils (single element only), but requires large computation times due to the flowfield solution method and grid resolution necessary for reliability [11].

- **LEWICE/UNS(NEARICE).** An unstructured-mesh derivative of LEWICE/NS, developed by Nielsen Engineering and Research of Mountain View, California. NEARICE was created to overcome problems with grid complexity for very convoluted shapes in LEWICE/NS that required excessive user interaction. The Euler/Navier-Stokes flow solution method captures flow separations and can predict aeroperformance of iced

configurations. Although currently under proprietary restriction by Nielsen, NEARICE will be made available in the future. A 3D equivalent is in development.

- **MSES/MICE.** A multi-element version of LEWICE based on the MSES airfoil design/optimization code written by Mark Drela and of the Massachusetts Institute of Technology. MSES is a 2D finite-volume Euler solver on an intrinsic streamline grid with an integral boundary layer calculation. Viscous-inviscid coupling captures flow separation, free transition, and turbulent reattachment over a wide range of Reynolds numbers and Mach numbers on multiple airfoil elements. This code suite is currently under development at MIT.<maybe Tom's thesis, to be published?>

- **LEWICE/X.** An experimental version of LEWICE intended to incorporate new physical models into existing LEWICE structure. Flowfield and trajectory modules are identical to baseline LEWICE. The energy balance and ice growth routines have been modified to include the growth of rime ice feathers in directions different from surface-normal. This code is currently under development at MIT and is the subject of this thesis.

## 2.2 Basic LEWICE Structure

LEWICE uses a Hess-Smith potential flow solver [4] coupled with a Thwaites-method integral boundary layer routine to calculate shape factors based on the external flow and determine the convective heat transfer coefficient distribution. The trajectory module integrates droplet trajectories using Langmuir's inertial/aerodynamic model [5] to determine the collection efficiency distribution. The ice accretion module uses the collection efficiencies and heat transfer coefficients to perform a mass and energy balance on each panel, determining the local freezing fraction distribution and resultant ice heights. Freezing fractions are calculated by using a Newton-Raphson iteration method to determine surface temperature; ice densities are found from Macklin correlation [6]. The



ice surface is then grown numerically and panels are distributed on or deleted from the new surface geometry according to several distribution and smoothness criteria. If the total ice shape is to be calculated in more than one timestep, the new geometry is then fed back into the flowfield module for recalculation (Figure 8).

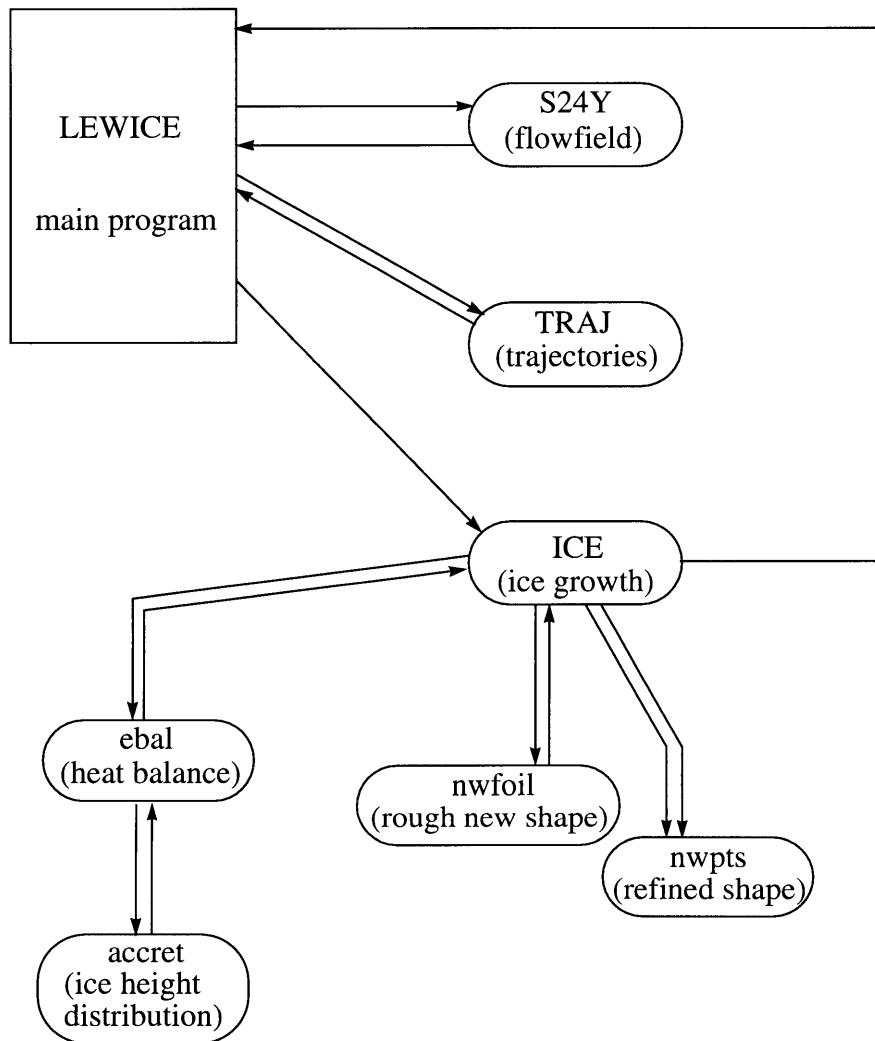


Figure 8. Flowcharting for LEWICE.

## 2.3 Physical Modeling of Ice Growth

The Messinger ice growth model implemented in LEWICE is detailed in [12], and will be summarized here so that the changes made to the model may be more readily understood.

After the flowfield properties and collection efficiency distributions have been calculated, the ice growth module performs a mass/energy balance on each control volume, beginning with the stagnation panel and moving aft on each side of the airfoil. The mass balance is simple and shown in Figure 9:

$$\dot{m}_c + \dot{m}_{rin} = \dot{m}_i + \dot{m}_{rout} + \dot{m}_e$$

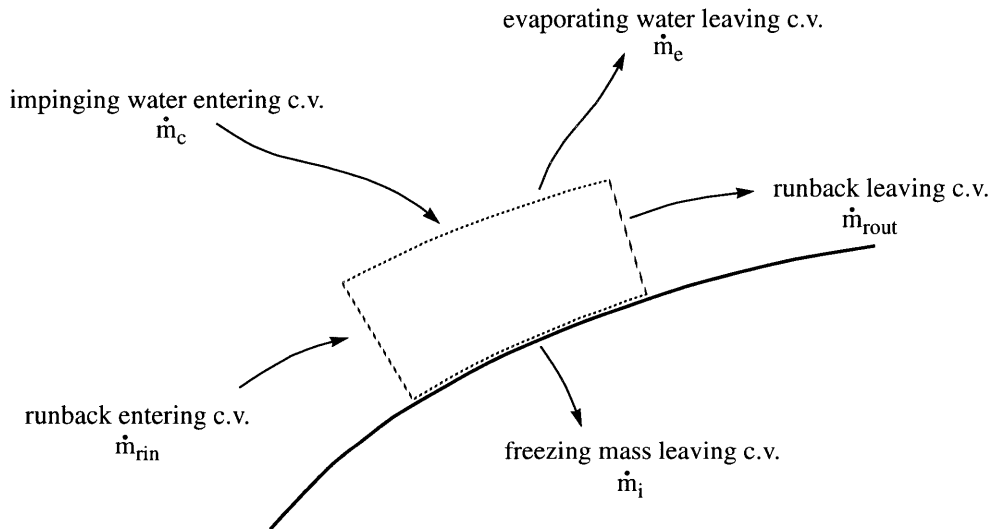


Figure 9. Mass balance for a typical control volume.

The energy balance is more complex due to the large number of energy flux terms for each control volume boundary. On the left-hand side of the equation are the incoming energy terms, associated with impinging and runback water. The impinging

contribution contains a thermal energy term and a stagnation enthalpy term:

$$q_{impinging} = \dot{m}_c \left[ C_{p(w,s)} (T_s - T_m) + \frac{V^2}{2} \right]$$

The runback into the control volume adds energy at the temperature and specific heat from the upstream panel:

$$q_{runback, in} = \dot{m}_{rin} [C_{pw, sur(i-1)} (T_{sur(i-1)} - T_m)]$$

There is a conduction term that defaults to a 1D conductive heat transfer value for heat loss across a boundary:

$$q_{conduction} = q_k \Delta s$$

The right hand side of the equation contains the terms that represent heat transfer out of the control volume. An evaporative heat transfer term is included for completeness, but is generally quite small:

$$q_{evaporating} = \dot{m}_e [C_{pw, sur} (T_{sur} + T_m) + L_v]$$

The freezing ice removes the latent heat of fusion as well as its state energy:

$$q_{freezing} = f(\dot{m}_c + \dot{m}_{rin}) [C_{pi, sur} (T_{sur} - T_m) - L_f]$$

The convective heat transfer term depends on the heat transfer coefficient and the local enthalpy at the edge of the boundary layer:

$$q_{convection} = HTC \left[ T_{sur} - T_e - \frac{V_e^2}{2C_{p, air}} \right] \Delta s$$

Finally, any unfrozen water leaving the control volume must be included in the balance:

$$q_{runback, out} = [(1-f)(\dot{m}_c + \dot{m}_{rin}) - \dot{m}_e] C_{pw, sur} (T_{sur} - T_m)$$

This energy is used again as  $q_{runback, in}$  for the next downstream panel.

The full form of the energy equation is then

$$\begin{aligned} \dot{m}_c \left[ C_{pw, s} (T_s - T_m) + \frac{V_\infty^2}{2} \right] + \dot{m}_{rin} [C_{pw, sur(i-1)} (T_{sur(i-1)} - T_m)] + q_k \Delta s = \\ \dot{m}_e [C_{pw, sur} (T_{sur} - T_m) + L_v] + f(\dot{m}_c + \dot{m}_{rin}) [C_{pi, sur} (T_{sur} - T_m) - L_f] + \\ HTC \left[ T_{sur} - T_e - \frac{V_e^2}{2C_{p, air}} \right] \Delta s + [(1-f)(\dot{m}_c + \dot{m}_{rin}) - \dot{m}_e] C_{pw, sur} (T_{sur} - T_m) \end{aligned}$$

This energy balance is performed over the entire surface, from the stagnation point aft for each side. The resulting freezing fraction distribution  $f(s)$  is used to calculate an ice height distribution. The calculated ice heights are added to the old geometry and a new airfoil is generated through a series of criteria including: panel angle change relative to neighboring panels; size change, both absolute and relative to neighboring panels; and smoothness. The new geometry can then be output or read back into the flowfield module for another timestep.

## 2.4 LEWICE Performance and Models

The above method predicts rime accretions with good accuracy. Some mixed ice accretions have been duplicated using unrealistically large sand-grain roughness values in the Thwaites-method boundary layer integration. LEWICE does not attempt to predict heat transfer-induced feather nucleation, and does not model ice growth in directions other than along surface normals.

# Chapter 3

## LEWICE/X

### 3.1 Physical Basis for Code Modification

#### 3.1.1 Heat Transfer Considerations

Icing tunnel tests were conducted by Hansman et al. [1] to determine roughness and rime feather effects on ice accretion. Cylinders were used as the test geometry. Close-up videotape of the accreting surface in mixed ice conditions showed feathers forming from initial surface roughness sites and being “backfilled” by glaze runback from the stagnation region, resulting in a mixed ice density. Small hornlike shapes resulted that grew in roughly the local particle impingement direction, or “into the flow”. These were designated Type A horns.

Roughness heat transfer studies were conducted at MIT in a low-speed wind tunnel to investigate the effect of surface roughness on local heat transfer [3]. Hemispherical roughness elements of various sizes were attached to a heated plate and viewed with an infrared camera. The results indicated that hemispherical elements have regions of enhanced heat transfer extending from roughly 1/4 diameter forward of the element center to several diameters aft. The amount of enhancement was between 150% and 250% in turbulent flow, and up to 600% in laminar flow. These data motivated an

improved ice growth model that captures the heat transfer enhancement properties of small roughness elements in order to model feather growth [2]. This model was to grow feathers from surface panels in roughly the impingement direction (see Section 3.1.2) and solid ice along surface normals. The feather and non-feather surfaces were separated, resulting in a two-surface ice accretion model.

### 3.1.2. Feather Growth Direction

Analysis of the ice shapes obtained for [1] show that the precise direction of feather growth varies somewhat with cloud and temperature conditions. Specifically, some Type A horns grew between the impingement and freestream directions. Ice tracings for cylinder tests conducted in NASA LerC's Icing Research Tunnel were examined. Growth angles were measured at the impingement limits and correlated with cloud conditions. This showed an linear variation with temperature and LWC. Further examination exposed a linear dependence of LWC-variation *rate* with temperature (Figure 10).

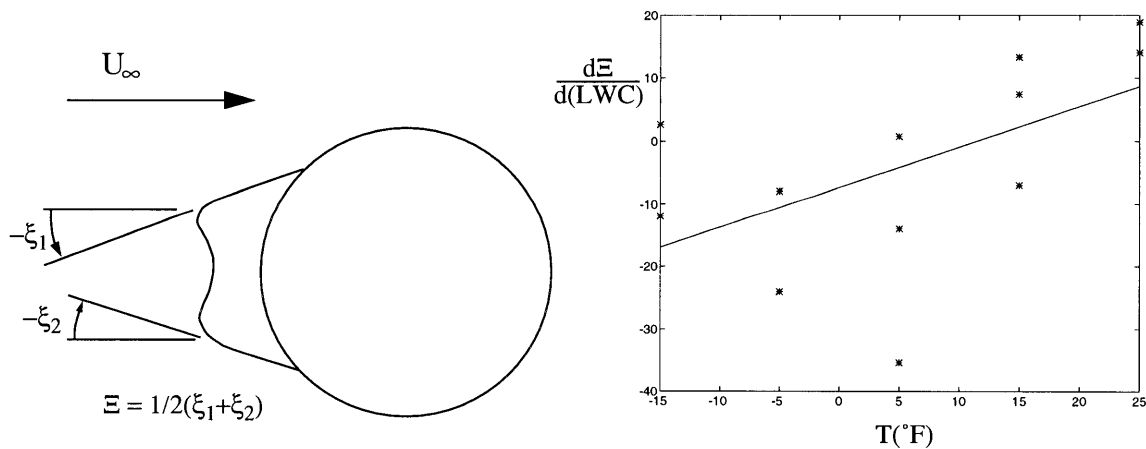


Figure 10. Results of feather growth angle analysis.  $\bar{\Xi}$  is measured in degrees from freestream direction. Each point on the plot represents a set of icing encounters for which LWC is the only variant. Solid line is a linear least-squares fit.

An assumed linear fit for the above plot gives the relation

$$\frac{\partial \Xi}{\partial (LWC)} = k_1 T + k_2$$

The coefficients  $k_1$  and  $k_2$  are in general functions of MVD. Integration yields

$$\Xi (T, LWC, MVD) = \Xi_0 + LWC (k_1 T + k_2)$$

where  $\Xi_0$  is the particle impingement angle. Since only two drop sizes were tested in [1], determination of the coefficients was not attempted. This model may vary for asymmetric geometries or configurations at an angle of attack. Due to time constraints, the model was not implemented in LEWICE/X. Growth angles for cases shown in Section 3.3 were set to match experimental shapes.

## 3.2 Description of Improved Ice Growth Model

LEWICE/X attempts to predict the extent of a feathered ice shape by modeling feather surface regions as continuous shapes as shown in Figure 11. It does not attempt to model individual feathers. In addition to the feather surface, LEWICE/X keeps track of a substrate surface grown in parallel with the feather surface. This accounts for any water that impinges in gaps between real feathers or runs back from upstream. The result is a dual-surface model of the total ice accretion. Type A horns are predicted with this method by allowing the substrate to prevent the nucleation of feathers or to overtake growing feathers.

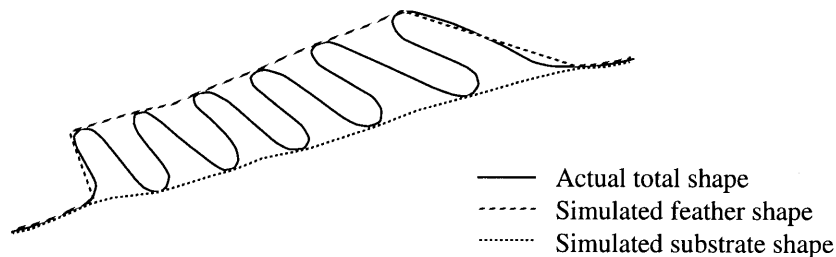


Figure 11. Feathers modeled as a continuous surface.

The feather accretion model proposed in [2] is implemented in four main subroutines with several smaller branches performing discrete tasks (Figure 12). The algorithm is a fairly simple permutation of the LEWICE algorithm, requiring the addition of several corrections to account for the new growth direction. The following description should be read with the understanding that the ice accretion is performed in a series of finite timesteps, and that some parameters are carried over to consecutive timesteps.

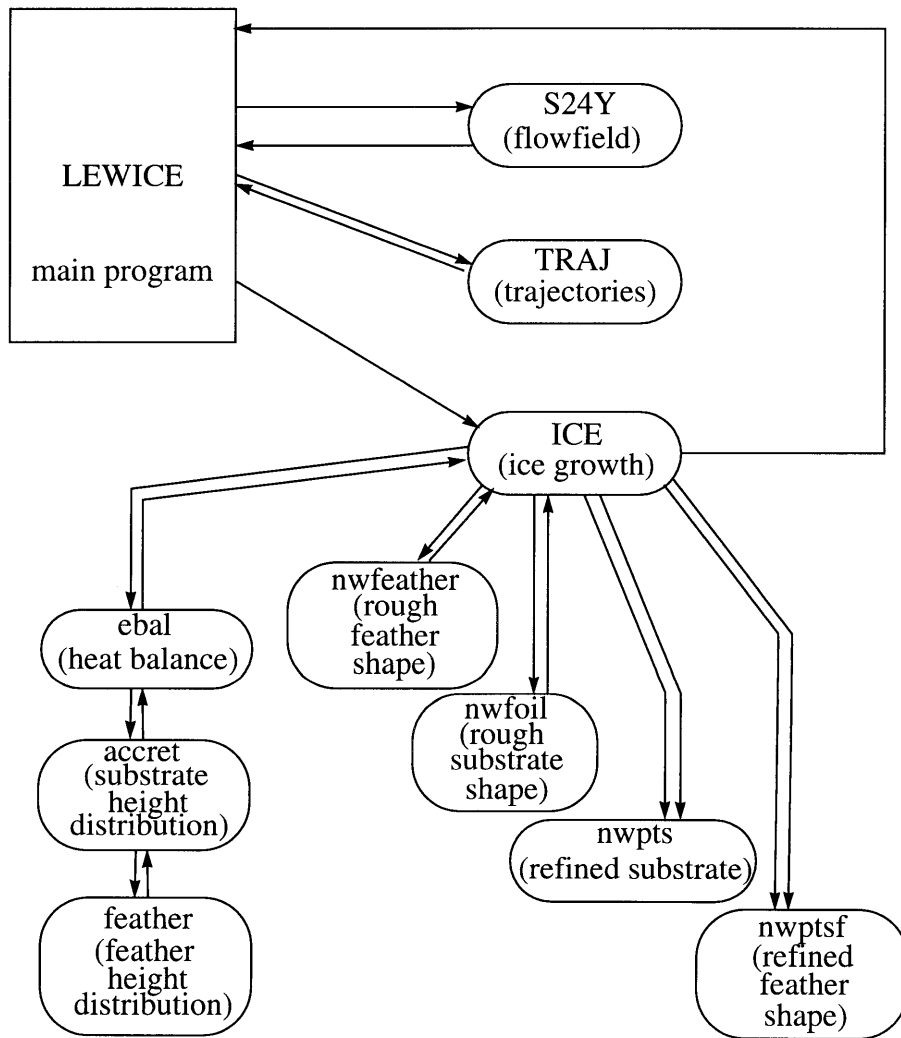


Figure 12. Flowcharting for LEWICE/X.



### 3.2.1. Thermodynamic Calculations

The ice accretion routine begins at the stagnation panel and works aft on the suction and pressure surfaces. An effective panel solidity factor models discrete feather regions. The solidity  $\sigma$  is defined to be the fractional projected area of physical feathers in the impingement direction and is shown graphically in Figure 13.

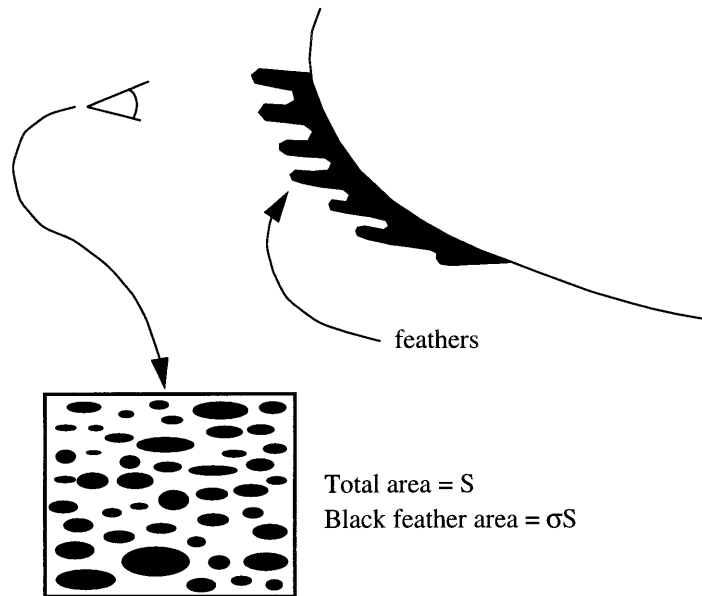


Figure 13. Solidity definition.

This scaling factor accounts for gaps between real feathers. These gaps influence the effective ice density for the improved model as well as the mass impinging on the feathers. Local solidity is almost certainly a function of feather height and spanwise opening angle, but there is no organized data on which to base conclusively a model.

The impinging mass flux on a feather panel is calculated to be

$$\dot{m}_f = \sigma \cdot \dot{m}_c = \sigma \cdot LWC \cdot V_\infty \cdot \beta$$

Subroutine *feather* enhances the convective heat transfer coefficient by a factor of  $e \cdot \sigma$ . The enhancement factor  $e$  accounts for roughness elements or feather tips protruding through the boundary layer, yielding higher than normal convective heat transfer coefficients [2,3]. Multiplication by the solidity is required because the enhanced heat transfer only occurs at the tips of the feathers. The remainder of the real surface has lower heat transfer values.

With the impinging mass scaled by  $\sigma$  and runback mass excluded from the calculation (since feathers can only grow from impinging droplets), the energy equation for the feather panel becomes

$$\dot{m}_f \left[ C_{pw,s} (T_{sur} - T_m) + \frac{V_\infty^2}{2} \right] + q_k \Delta s = f_f (\dot{m}_f) [C_{pi,sur} (T_{sur} - T_m) - L_f] + \sigma e \cdot HTC \left[ T_{sur} - T_e - \frac{V_e^2}{2C_{pair}} \right] \Delta s + [(1 - f_f) \dot{m}_f] C_{pw,sur} (T_{sur} - T_m)$$

The feather freezing fraction is calculated from this equation by setting  $T_{sur}$  equal to  $T_m$ , yielding

$$\frac{\dot{m}_f V_\infty^2}{2} + q_k \Delta s = \sigma e \cdot HTC \left[ T_m - T_e - \frac{V_e^2}{2C_{pair}} \right] - f_f \dot{m}_f L_f$$

If the freezing fraction based on this equation is less than 1, the heat transfer is not high enough to support dry growth, and the freezing fraction and ice growth calculations must be re-performed with unenhanced heat transfer and the full incoming mass (impinging + runback). Because of the binary nature of the feather freezing fraction (1 or 0), the otherwise crude approximation that  $T_{sur} = T_m$  may be made without ill consequence.

### 3.2.2. Feather Growth

If the enhanced-HTC freezing fraction is found to be equal to 1, the impinging mass is grown on the feather surface as a parallelogram (Figure 14). Its “height”, defined in the direction of the local surface normal, is calculated as

$$h_{feather} = \frac{\dot{m}_f \Delta t}{\sigma \cdot \rho_{rime}} = \frac{\dot{m}_c \Delta t}{\rho_{rime}}$$

It is interesting to note that the final feather height is independent of the solidity, and is equal to the height that would result if the entire impinging mass for the panel were frozen as rime ice and grown normal to the surface. This is consistent with experimental observations indicating that for constant thermodynamic conditions the feather growth rate is dependent only on impinging mass flux. In addition, for icing conditions in which the normal LEWICE method would predict purely rime growth, the feather heights and resulting iced geometry should be similar to normal LEWICE results.

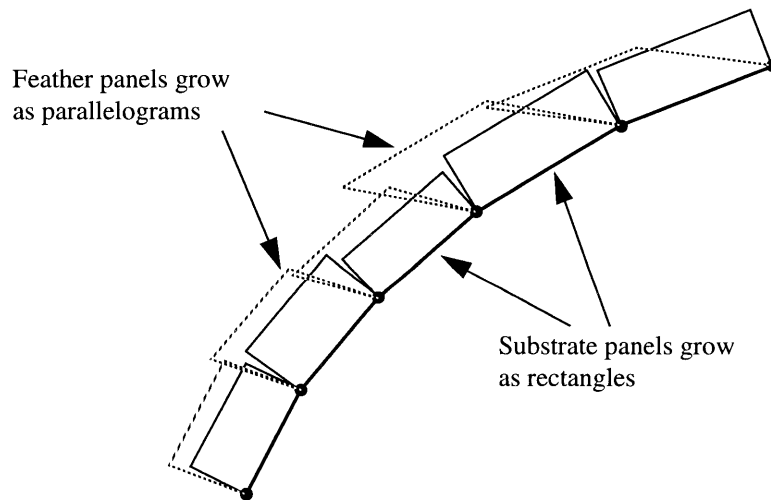


Figure 14. Feather vs. substrate growth directions.

### 3.2.3. Substrate Growth

Once the feather height is determined, the substrate height is calculated using the unenhanced heat transfer coefficient and the remaining incoming water (impinging + runback). This calculation generates a secondary surface underneath the feather surface, hence the name substrate. The energy balance for this surface is slightly different from the original LEWICE equation, since the impinging mass is reduced and the energy lost to feather growth must be taken into account. The resulting equation is

$$\begin{aligned} \dot{m}_s \left[ C_{pw, s} (T_s - T_m) + \frac{V_\infty^2}{2} \right] + \dot{m}_{rin} [C_{pw, sur(i-1)} (T_{sur(i-1)} - T_m)] + q_k \Delta s = \\ \dot{m}_e [C_{pw, sur} (T_{sur} - T_m) + L_v] + f_s (\dot{m}_s + \dot{m}_{rin}) [C_{pi, sur} (T_{sur} - T_m) - L_f] + \\ HTC \left[ T_{sur} - T_e - \frac{V_e^2}{2C_{p, air}} \right] \Delta s + [(1 - f_s) (\dot{m}_s + \dot{m}_{rin}) - \dot{m}_e] C_{pw, sur} (T_{sur} - T_m) - \\ \dot{m}_f [C_{pi, sur} (T_{sur} - T_m) - L_f] \end{aligned}$$

where

$$\dot{m}_s = \dot{m}_c (1 - \sigma)$$

and  $f_s$  is the freezing fraction of the incoming mass for the substrate panel. An initial estimate of the substrate freezing fraction is made with the method used for calculating  $f_f$ . Fine resolution of  $f_s$  and  $T_{sur}$  is achieved with a Newton-Raphson iteration performed on the fully nonlinear accretion equation. The substrate ice grows as a rectangle from the solidity-reduced mass into the volume not occupied by feathers:

$$h_{substrate} = \frac{[(1 - \sigma) \dot{m}_c + \dot{m}_{rin}] \Delta t}{\rho_{substrate} (1 - \sigma)}$$

The resulting substrate panel is compared with the feather panel that was just

calculated.

Experimental observations show that near stagnation in Type A horn conditions, dry roughness elements are usually covered or splashed with unfrozen water that negates their heat transfer qualities and prevents feather growth in that region. This is modeled in LEWICE/X by allowing two possibilities when the feather and substrate heights are compared:

a) Substrate does not overtake the feather panel (previous timesteps included); the relevant panel quantities are written to permanent arrays and any remaining water is passed to the next downstream panel. the feather growth calculation is allowed to continue.

b) Substrate overtakes the feather; the previous feather prediction was in error. The feather height for the current panel and timestep is set to zero and the panel is recalculated using the normal LEWICE method.

If there was previously no feather growth at this panel (this is the case for all panels at the first timestep), a runback water film height is calculated and compared to the roughness element height. If the film height exceeds the roughness level, the panel is recalculated using the normal LEWICE method. This models water the water film washout described in Section 1.4.

### 3.2.4. Calculation of Iced Geometry

After the feather and substrate heights are computed for the entire airfoil, it is necessary to compute new substrate and feather shapes based on the results. Since LEWICE already does this for the substrate shape, the new feather shape is easily mapped according to the point distribution of the substrate in a four-step process.

- **Re-panel substrate surface.**

The new shape calculation for the substrate is performed first, and the feather

shape will be mapped to fit it. The new substrate geometry is calculated by first shifting each panel outward by its calculated ice height, then redistributing points to smooth the surface [12].

• **Accrete feather surface.**

The first step in the calculation of the new feather shape is a rough determination of the new surface in subroutine *nwfeather*. Each panel is shifted outward by the calculated feather height, but instead of shifting normal to the surface, the feather panel is shifted in the local growth direction. Any point on the feather surface has two potential new locations based on the feather heights to either side, so the midpoint between the two candidates is chosen as the new point (Figure 15).

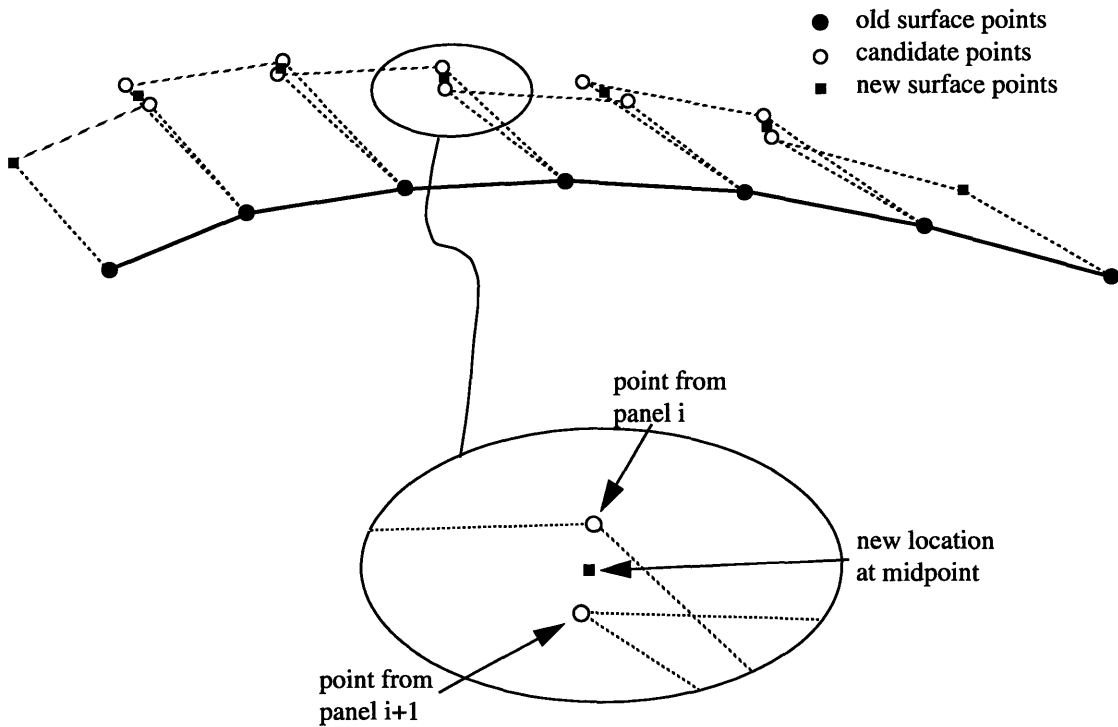


Figure 15. Initial repaneling method for feather geometry.

• **Identify non-feather regions.**

Figure 16 shows the results of the initial feather accretion starting from a clean

surface. If the number of panels were to be held constant and each  $i$ th feather panel corresponds to the  $i$ th substrate panel, the feather shape would not be closed; therefore a few additional panels are necessary at the ends of each feather region to close the shape. If each ‘virtual’ panel is marked and handled specially in subsequent timesteps, a one-for-one correspondence between feather and substrate panels is maintained.

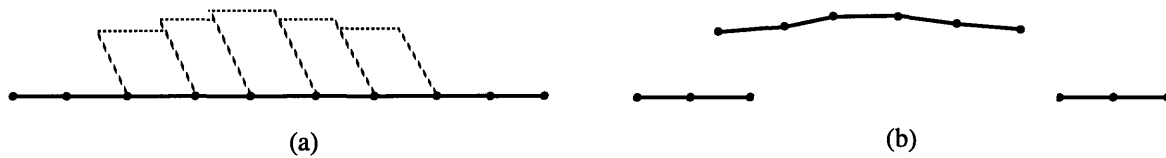


Figure 16. (a) Initial surface with calculated feather parallelograms. (b) Updated surface with number of panels held constant.

Outside feather regions, points on the feather shape are identical to points on the substrate shape (including those that have grown ice; the feather geometry will be passed to the flowfield module in the next timestep and should contain points for whichever shape is locally more external). Subroutine *nwptsf* scans the updated feather geometry for endpoints of feather regions. When an endpoint is located, a line is drawn aft in the local growth direction, and a substrate panel is located that intersects this line. The nearest substrate point is chosen to correspond to the feather region endpoint (Figure 17). This is repeated until a substrate point has been found to correspond with each endpoint. All feather points outside these regions are known to be identical to the re-paneled substrate and may be written to a new geometry array. The total number of points in the new feather shape will be  $N+2b$ , where  $N$  is the number of points in the new substrate shape and  $b$  is the number of feather regions.

- **Re-panel feather regions.**

Since a one-for-one correspondence between feather and substrate panels is desired, the best solution is to re-panel the feather regions so they contain the same number

of panels as the underlying substrate. A point density distribution is calculated for the substrate and mapped onto the feather shape so that each panel in the underlying substrate corresponds to a feather panel in the growth region. This method distributes feather points so that surface distance percentages are identical from feather to substrate (that is, a substrate point 1/3 of the way across a feather region will correspond to a feather point 1/3 of the way across that region, regardless of any difference in total surface distance).

The presence of several 'virtual' panels necessary to close the feather shape complicates only the ice growth routines. The flowfield and trajectory modules work exclusively with the feather geometry. The ice growth routines work with the substrate geometry and have loops to determine if a virtual panel has been encountered in the feather shape. If so, it is ignored and calculations continue with the next downstream feather panel. All incoming water for virtual panels is passed downstream. The one-for-one panel correspondence between the feather and substrate shapes is preserved (Figure 18).



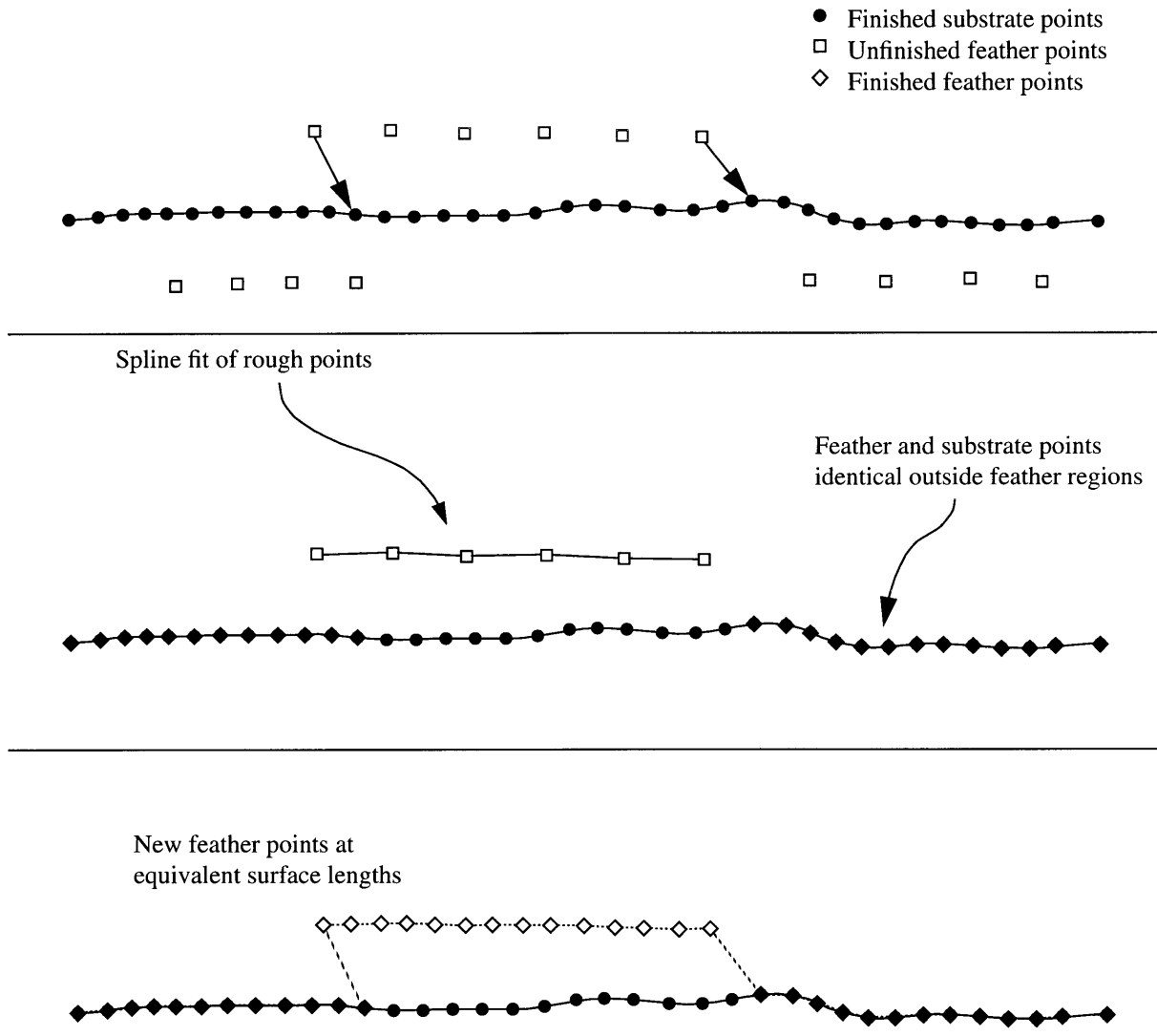


Figure 17. New feather shape point distribution based on substrate distribution.

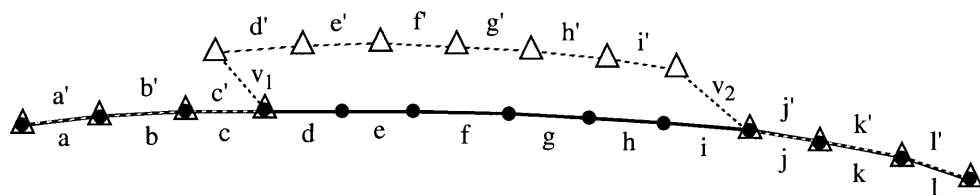


Figure 18. Feather-substrate panel correspondence showing virtual panels  $v_1$  and  $v_2$ . Unprimed letters are substrate panels. Primed letters are feather panels.

### 3.3 LEWICE/X Performance

A number of test runs were performed to determine the effect of feather solidity  $\sigma$  on the resulting iced geometry. Increasing  $\sigma$  reduces the amount of water reaching the substrate surface. This decreases the substrate height as  $\sigma$  is increased, but otherwise there should be little effect. The results of this parametric study, shown in Figure 19, support this. Apart from small changes in the substrate, shapes for varying  $\sigma$  are similar.

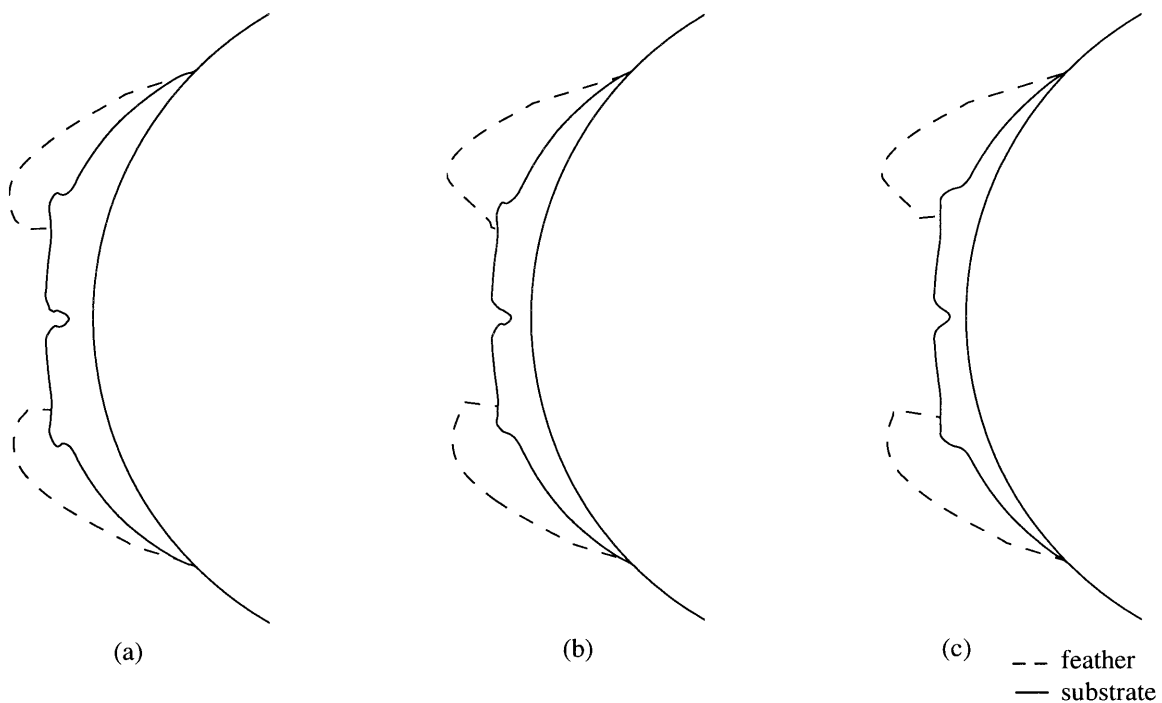


Figure 19. Solidity sweep for  $V=200$  mph,  $LWC=0.5$  g/m<sup>3</sup>,  $MVD=15$   $\mu$ m,  $T=25^\circ$ F. 12 minute accretions. (a)  $\sigma = 0.4$ ; (b)  $\sigma = 0.5$ ; (c)  $\sigma = 0.6$ .

A parameter sweep was also performed for the initial roughness element height,  $k_x$ . The sensitivity of the forward feather limits to initial roughness height is apparent from the shapes in Figure 20. Yamaguchi et al. [14] have suggested that the change in accretion behavior from glaze ice to feathers occurs at the boundary layer transition location. The results of this parameter sweep suggest that the behavior transition is related more directly to surface roughness.

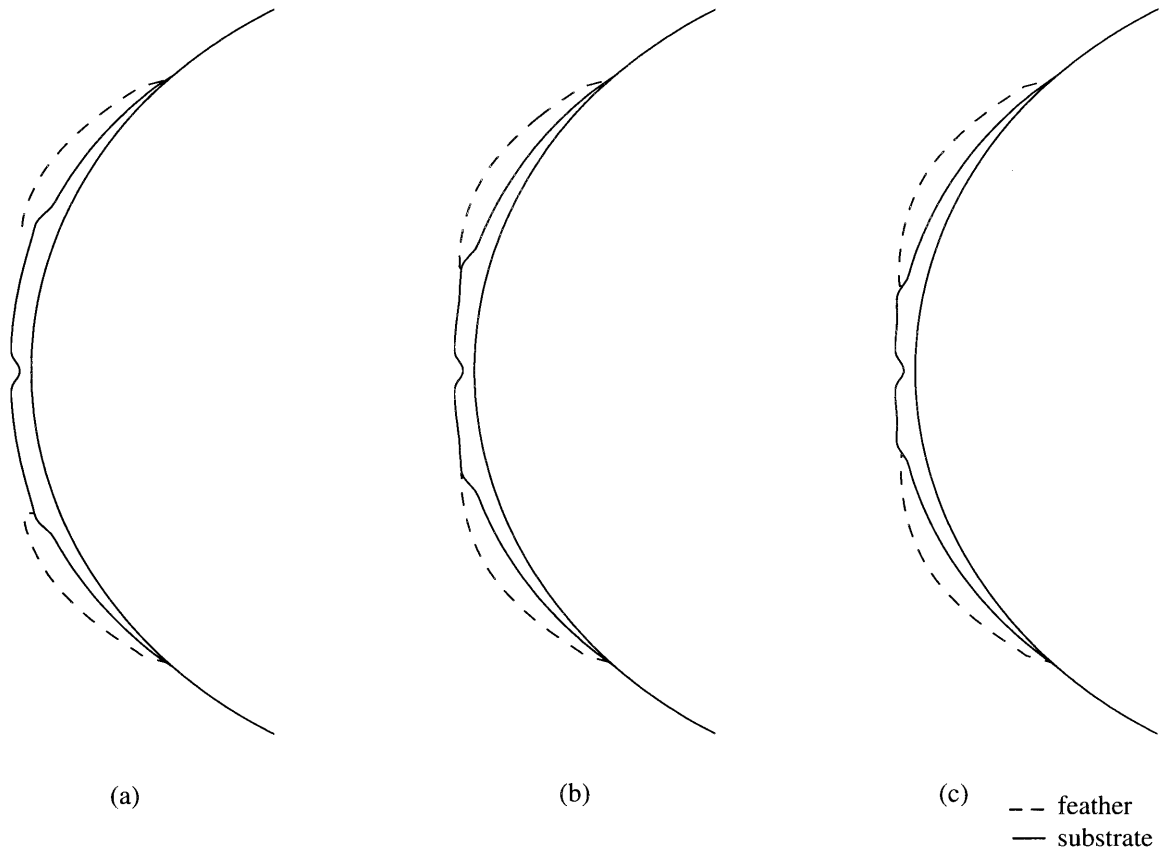


Figure 20. Roughness sweep for  $V=200$  mph,  $LWC=0.5 \text{ g/m}^3$ ,  $MVD=15 \text{ m}$ ,  $T=25^\circ\text{F}$ .  
 4 minute accretions. (a)  $x_k = 0.1 \text{ mm}$ ; (b)  $x_k = 0.5 \text{ mm}$ ; (c)  $x_k = 1.0 \text{ mm}$ .

Figures 21 and Figure 22 show a comparison between LEWICE/X and LEWICE/Beta for a mixed accretion and a Type A horn accretion, respectively. Several parameters were varied to achieve overall shape agreement. The feather solidity  $\sigma$  was set to 0.4 for both cases shown to reduce runback aft of the feather regions (no runback is ever seen aft of feathers in real accretions). This value was based on an estimated final  $\sigma$  of 0.8 from photographs of the real accretion. The boundary layer transition location was moved to the stagnation point, making the flowfield and heat transfer fully turbulent. This increased the ice thickness in the stagnation region to match the experimental value. An effective feather nucleation element height was varied to control the forward feather limits

according to the runback overgrowth mechanism described in Section 1.4. Initial element heights of 0.25 mm yielded matched feather limits in both cases. Single-timestep simulations were used.

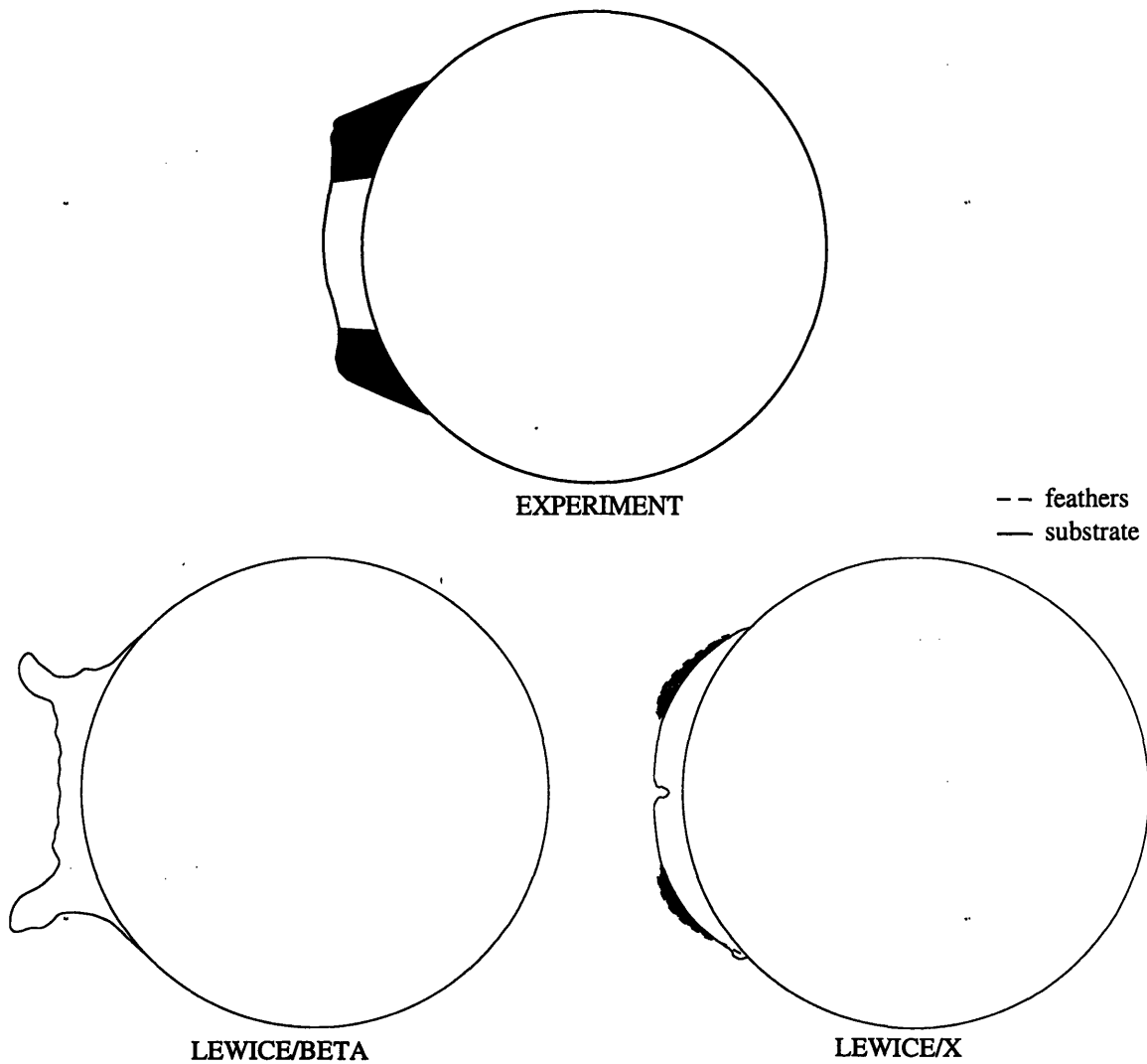


Figure 21. Accretions on 3.5" diameter cylinders.  $V=200$  mph;  $LWC=0.32$  g/m<sup>3</sup>;  $MVD=15$  m;  $Temp.=15^{\circ}F$ . 12 minute accretion. Shaded areas represent feather regions.

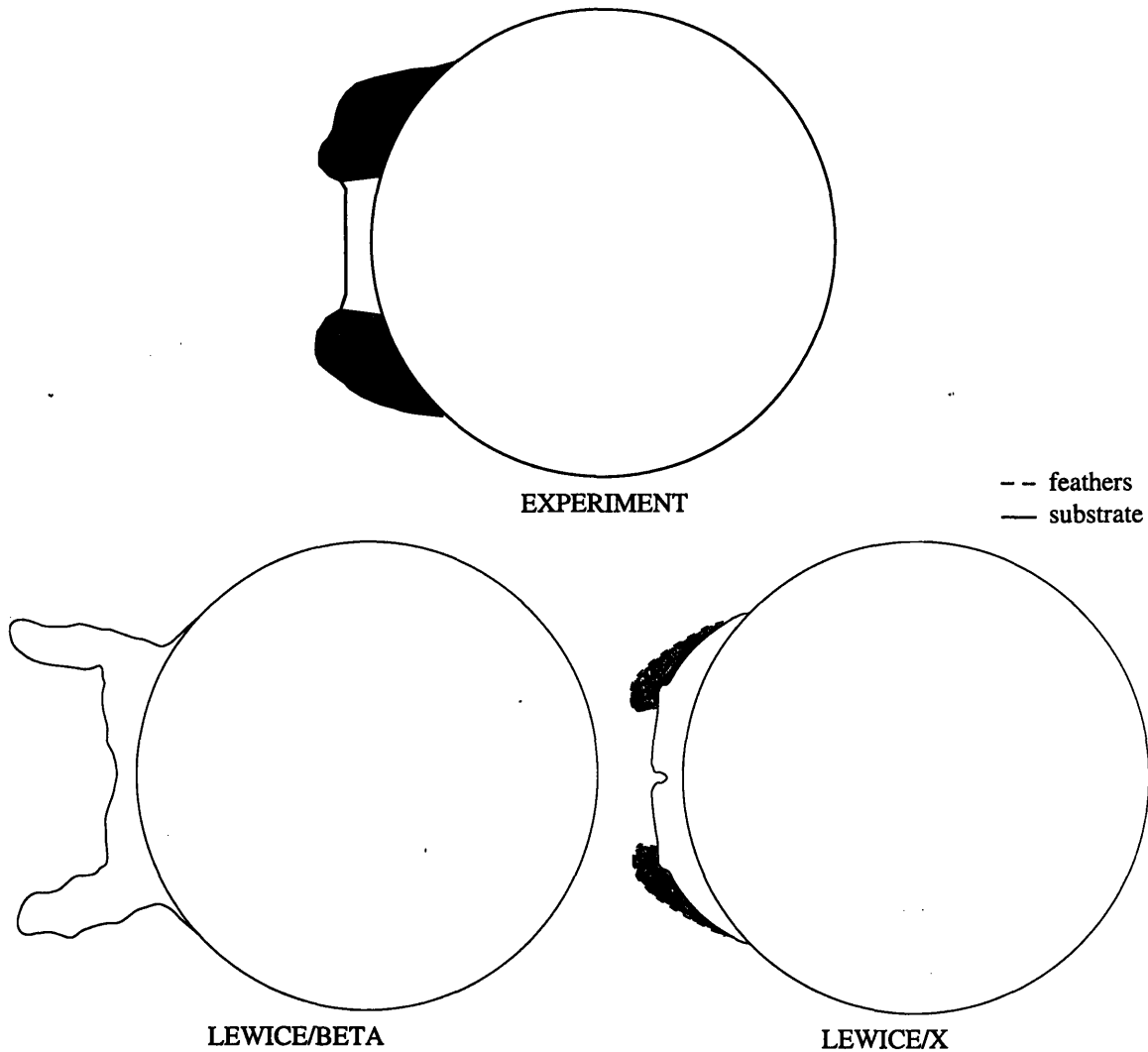


Figure 22. Accretions on 3.5" diameter cylinders.  $V=200$  mph;  $LWC=0.5 \text{ g/m}^3$ ;  $MVD=15$  m;  $\text{Temp.}=25^\circ\text{F}$ . 12 minute accretion. Shaded areas represent feather regions.

The experimental shape in Figure 21 shows little horn growth but distinct feather and glaze regions. LEWICE/X captures these feather regions well. Unmodified LEWICE predicts very wet glaze accretion and Type B horns for the same input parameters. The shape in Figure 22 is a more distinct Type A horn accretion. LEWICE/X correctly predicts the horn growth whereas unmodified LEWICE again predicts glaze accretion.

In both of these cases LEWICE/X underpredicts feather growth near the

impingement limits. The slight variance in feather height may be caused by iced area lost due to overlap of adjacent feather parallelograms, or by an inaccurate solidity model near the impingement limits.

# Chapter 4

## Conclusions

### 4.1 Summary

LEWICE/X has been developed and implemented to simulate rime feather growth on icing surfaces and resultant Type A horn formation. The physical phenomena modeled include:

- heat transfer enhancement at surface contamination sites and roughness sites;
- rime feather growth resulting from local heat transfer enhancement;
- runback-driven feather prohibition near stagnation;
- ice growth in non-surface-normal directions.

These physical models are implemented in a dual-surface variant of the Messinger control volume model of ice accretion. Impinging droplets are separated from runback and, if convective heat transfer is high enough, grown on a separate geometry approximately in the local impingement directions. Runback is grown as a substrate of the feather shape. Calculated iced geometries agree well with experimental shapes. Unmodified LEWICE incorrectly predicts glaze ice growth for two cases tested.

Experimental data suggests a variation in the direction of feather growth with cloud conditions. Investigation of empirical data revealed a linear dependence of the rate of change of feather growth angle with respect to LWC on temperature. Drop size is definitely a factor as well, but a limited range of MVD in the empirical data prevented a

concrete determination of its effect.

## 4.2 Observations of LEWICE/X Performance

- Values of initial surface roughness and heat transfer enhancement used to generate shape predictions with good agreement are physically realistic. Type A horns can be predicted without the artificial heat transfer increase required by LEWICE to generate the same shapes.

- The forward extent of feather regions on either side of the stagnation zone is influenced by the initial roughness element height. Larger initial roughness heights moved the feather regions closer to the stagnation point. This suggests that the real feather limits may also be controlled by initial contaminant size, not by turbulent transition as suggested by Yamaguchi et al. [14].

- LEWICE/X underpredicts feathers near the impingement limits for the two cases shown. This could be caused by iced area lost during re-paneling, or by an inaccurate model for the fraction of impinging droplets growing into feathers.



# References

- [1] Hansman, R. J., Breuer, K.s., Hazan, D., Reehorst, A., and Vargas, M. Close-up Analysis of Aircraft Ice Accretion. AIAA 93-0029, 1993.
- [2] Hazan, Didier. Improved Ice Growth Modeling Based on Close-up Analysis of Aircraft Ice Accretion. M.S. Thesis, Massachusetts Institute of Technology, June 1993.
- [3] Henry, R., Hansman, R. J., and Breuer, K. S. Measurement of Heat Transfer Variation on Surface Roughness Elements Using Infrared Techniques. AIAA 94-0801, 1994.
- [4] Hess, J. L., and A. M. O. Smith. Calculation of Potential Flow About Arbitrary Bodies. *Progress in Aeronautical Sciences*, Vol. 8 pp. 1-138, 1967.
- [5] Langmuir, I., and Katharine B. Blodgett. A Mathematical Investigation of Water Droplet Trajectories. Army Air Force Technical Report No. 5418, 1946.
- [6] Macklin, W. C. The Density and Structure of Ice Formed by Accretion. *Quarterly Journal of the Royal Meteorological Society*, Vol. 88: pp. 30-50, 1962.
- [7] Messinger, B. L. Equilibrium Temperature of an Unheated Icing Surface as a Function of Airspeed. *Journal of the Aeronautical Sciences*, Vol. 20: pp. 29-42, 1953.
- [8] Olsen, William. Survey of Aircraft Icing Simulation Test Facilities in North America. NASA TM 81707, 1981.
- [9] Perkins, P., and W. Rieke. Aircraft Icing Problems - After 50 Years. AIAA 93-0392, 1993.
- [10] Potapczuk, M. G., and J. J. Reinmann. Icing Simulation: A Survey of Computer Models and Facilities. NASA TM 104366, 1991.
- [11] Potapczuk, M. G. LEWICE/NS User's Manual. Unpublished.
- [12] Ruff, A. G., and M. Brian Berkowitz. User's Manual for the NASA Lewis Ice Accretion Prediction Code (LEWICE). NASA CR 185129, 1990.
- [13] Yamaguchi, Keiko. Improved Ice Accretion Prediction Techniques Based on Experimental Observations of Surface Roughness Effects on Heat Transfer. M.S. Thesis, Massachusetts Institute of Technology, May 1990.
- [14] Yamaguchi, Keiko, and R. J. Hansman. Heat Transfer on Accreting Ice Surfaces. AIAA 90-0200, 1990.